Hindawi
Advances in Civil Engineering
Volume 2018, Article ID 1356027, 16 pages
https://doi.org/10.1155/2018/1356027

Research Article

Flexural Design and Analysis of Composite Beams with Inverted-T Steel Girder with Ultrahigh Performance Concrete Slab

Wonchang Choi,[1] **Youngcheol Choi**,[2] **and Sung-Won Yoo**[2]

[1]*Department of Architectural Engineering, Gachon University, Seongnam-si 13120, Republic of Korea*
[2]*Department of Civil and Environmental Engineering, Gachon University, Seongnam-si 13120, Republic of Korea*

Correspondence should be addressed to Sung-Won Yoo; imysw@gachon.ac.kr

Received 28 December 2017; Accepted 6 May 2018; Published 13 June 2018

Academic Editor: Evangelos J. Sapountzakis

This study intends to improve the efficiency of the composite beam combining a slab made of steel fiber-reinforced ultrahigh performance concrete (UHPC) and a steel girder without top flange. To that goal, the experiment is conducted on 24 composite beams fabricated with varying compressive strength of UHPC, steel fiber content, stud spacing, and slab thickness to evaluate the behavior of the studs and the flexural behavior of the composite beam combining the UHPC slab and the inverted-T steel girder. The experimental results show the test members developed sufficient ductile behavior with respect to the slip limit of 6 mm stipulated in Eurocode-4 and regardless of the considered test variables. The experimental ultimate horizontal shear force is seen to be clearly larger than the static strengths of the stud predicted by Eurocode-4 and AASHTO-LRFD. Improved design formulae for the composite beam shall be derived to reflect the UHPC slab thickness.

1. Introduction

In order to overcome the low tensile and flexural strengths of conventional concrete, study is being actively conducted worldwide on steel fiber-reinforced ultrahigh performance concrete (UHPC) developing compressive strength higher than 120 MPa through the admixing of steel fiber in high performance concrete [1–3]. While, the flexural behavior of fiber-reinforced concrete can be influenced by specimen size, concrete casting method, and support devices [4]. Such steel fiber reinforced UHPC is known to present improved deflection, flexural strength, and postcracking ductile behavior compared to conventional concrete.

Composite structures are probably the most appropriate application enabling to take full advantage of the outstanding properties of UHPC, and various solutions combining a UHPC slab and a steel girder were successfully developed [5, 6]. In addition, numerical expression for flexure of UHPC beam has been successfully derived by the strain compatibility relation [7].

Yoo and Yoon [8] carried an extensive review for the behavior of various UHPFRC structures under different loading conditions, such as flexure, shear, torsion, and high-rate loads (impacts and blasts), with practical applications of UHPFRC in architectural and civil structures.

Among the latest achievements and to increase the economy in the material, Europe through the European Commission EUR 25321 developed the preco-beam, a composite beam combining a UHPC deck and an inverted-T steel girder of which the top is worked to have puzzle, fin or clothoidal dowel shape [9]. This dowel shape is obtained by oxycut of the web that may affect the fatigue behavior of steel [10]. Following the same idea and in order to ease the fabrication of the composite beam and to prevent this fatigue problem, the composite beam combining a slab made of steel fiber-reinforced UHPC and a steel girder without the top flange shown in Figure 1 was proposed [11, 12]. This composite beam was conceived considering the fact that the top flange of the steel girder might be superfluous when the composite beam is formed by composing a UHPC slab with the steel girder considering the high stiffness developed by the UHPC slab and that the shear connector can fulfill the role of the top flange of the steel girder. However, in the configuration shown in Figure 1, the studs needed for the

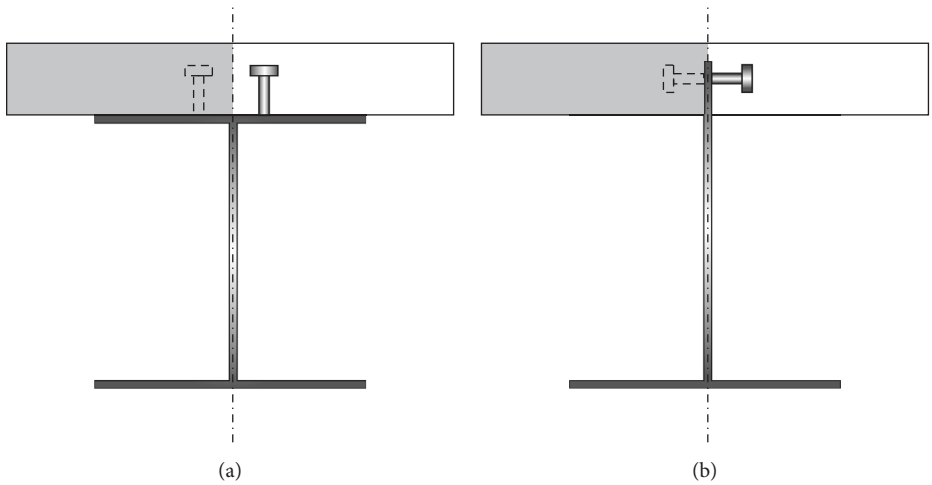

Figure 1: Configuration of conventional composite beam (a) and composite beam with inverted-T girder (b) [12].

Table 1: Physical properties of steel fiber per UHPC mix.

Design strength of UHPC (MPa)	Density (kg/m^3)	Length (mm)	Yield strength (MPa)	Volume fraction with respect to concrete (%)	
				ϕ19.5 mm	ϕ16.3 mm
120	7,800	13	2,500	1.0	—
150	7,800	13	2,500	1.0	0.5
180	7,800	13	2,500	1.0	0.5

composition of the steel girder with the UHPC slab must be disposed in the web of the girder because of the absence of the upper flange.

In a previous paper [12], the authors presented an experimental and analytical study on the flexural behavior of the proposed composite beam using the inverted-T steel girder and slabs made of UHPC with compressive strength higher than 180 MPa and considering the stud spacing and slab thickness as variables. The experimental results obtained from 8 composite beam specimens made it possible to recommend stud spacing ranging between 100 mm and 2 to 3 times the thickness of the slab. Considering that there is still no clear agreement on the limit compressive strength defining UHPC and that this compressive strength will affect significantly the behavior of the proposed composite beam, the present paper examines experimentally the behavioral characteristics of the shear connection and the flexural behavior of the composite beam based upon the results of a series of tests on 24 composite beam specimens with a inverted-T steel girder and steel fiber-reinforced UHPC slab considering the compressive strength of UHPC, the mix ratio of steel fiber, the stud spacing, and slab thickness.

2. Experimental Program

2.1. Material and Test Setup. Three compressive strengths of 120, 150, and 180 MPa are adopted as design strength of UHPC. UHPC samples were extracted during the fabrication of the flexural test members to perform compressive and tensile material tests for the establishment of the material models. The steel fibers have length of 19.5 and 16.3 mm and are admixed with respective volume fractions of 1.0% and 0.5% according to the considered mix. Table 1 arranges the physical properties of the steel fibers for each of the UHPCs considered in this study.

2.2. Bending Test of Composite Beam Specimens

2.2.1. Test Variables and Shape of Specimens. A total of 24 specimens were fabricated considering the compressive strength of UHPC (120, 150, and 180 MPa), the UHPC slab thickness (50 and 100 mm), and the stud spacing (50, 100, 200, and 400 mm) as test variables. Table 2 lists the test members with their designation and corresponding characteristics. Figure 2 describes the sectional dimensions and details of the test members.

The slab thickness is selected as a test variable to examine the effect of the embedment depth of the shear connector welded to the girder web on the composite behavior. The stud spacing is changed to derive the appropriate spacing enabling to secure the performance of the composite beam with the inverted-T steel girder. Finally, the compressive strength of UHPC and the mix ratio of steel fiber are chosen as test variables to examine the flexural behavior of the composite beam according to the compressive and tensile strength of UHPC [13, 14]. For the 120 MPa and 150 MPa test members, Figure 2 presents the original cross section (Figure 2(b)) and the modified cross section (Figure 2(c)). The modified cross section corresponds to some fabrication error in the dimension of the bottom flange of the steel girder, which was fabricated with a width shorter by 3 mm. This small fabrication error resulted in nonnegligible

Table 2: Designation and characteristics of composite beam members.

Designation of test member	Compressive strength of UHPC (MPa)	Volume fraction of steel fiber (%)	Slab thickness (mm)	Stud spacing (mm)	Dimensions of steel girder	Moment of inertia (mm^4/m)
120f-50-50	120	19.5 mm–1.0%	50	50	Figure 2(b)	648,204,096
120f-50-100				100		608,431,093
120f-50-200				200		606,338,700
120f-50-400				400	Figure 2(c)	624,077,520
120f-100-50			100	50		668,005,509
120f-100-100				100	Figure 2(b)	631,827,808
120f-100-200				200		629,097,682
120f-100-400				400	Figure 2(c)	644,004,858
150f-50-50	150	19.5 mm–1.0% + 16.3 mm–0.5%	50	50	Figure 2(b)	614,037,639
150f-50-100				100		577,958,206
150f-50-200				200		571,715,499
150f-50-400				400		584,448,794
150f-100-50			100	50		633,091,651
150f-100-100				100		598,844,031
150f-100-200				200		593,981,057
150f-100-400				400		604,406,484
180f-50-50	180	19.5 mm–1.0% + 16.3 mm–0.5%	50	50	Figure 2(d)	302,871,348
180f-50-100				100		302,111,136
180f-50-200				200		307,221,675
180f-50-400				400		311,096,506
180f-100-50			100	50		331,538,400
180f-100-100				100		326,779,611
180f-100-200				200		326,036,138
180f-100-400				400		324,346,281

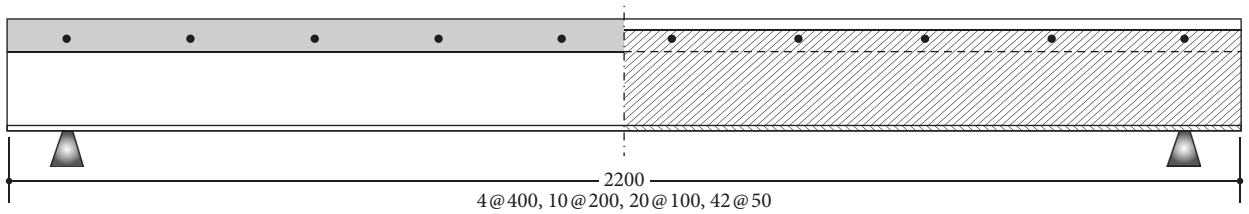

(a)

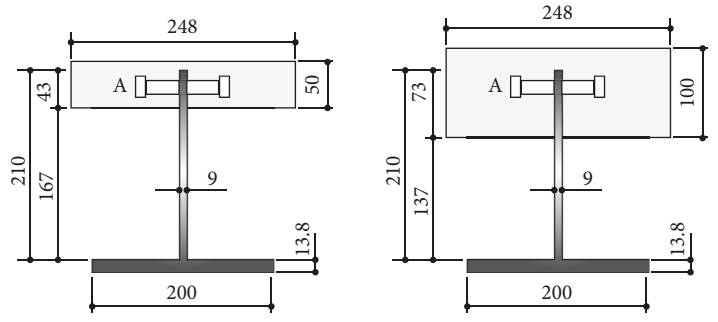

(b)

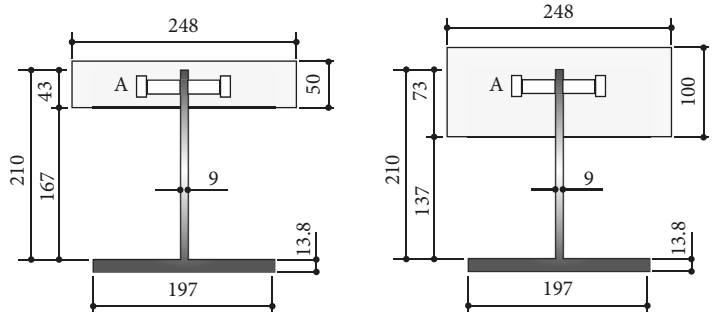

(c)

Figure 2: Continued.

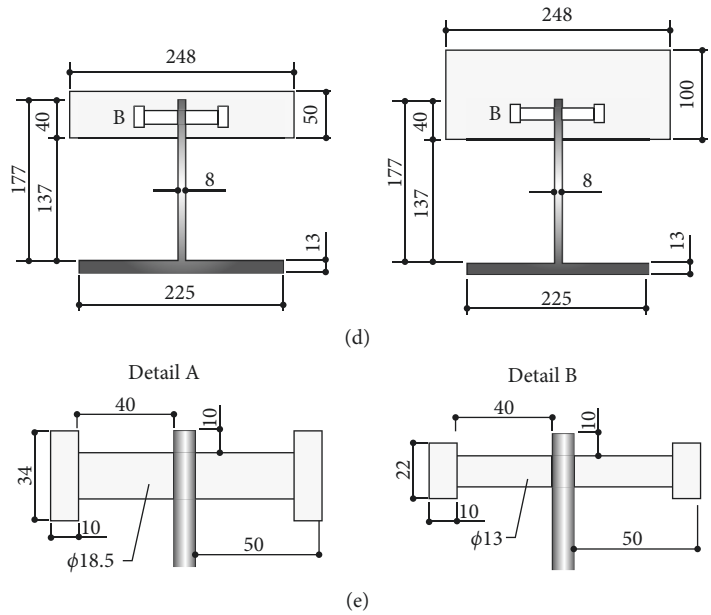

Figure 2: Sectional dimensions and details of test members (unit: mm). (a) Overall dimensions of composite beam members; (b) original 120 MPa and 150 MPa test members; (c) modified 120 MPa and 150 MPa test members; (d) 180 MPa test members; (e) details of studs for 120 MPa and 150 MPa members (left) and for 180 MPa members (right).

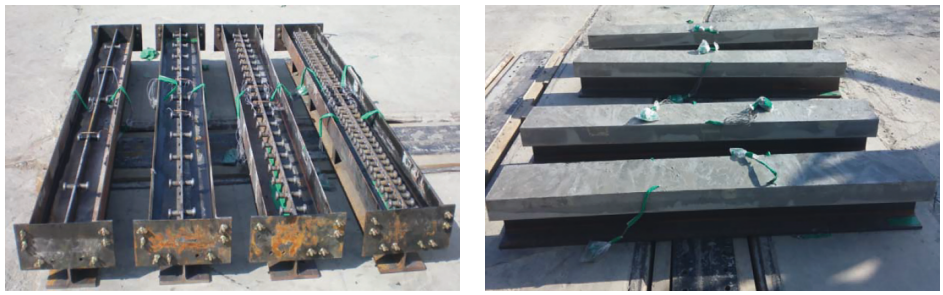

Figure 3: Fabrication of the composite beam with inverted-T steel girder. (a) Inverted-T steel girder with steel form: stud spacing of 400, 200, 100, and 50 mm from left to right. (b) Completed composite beams: stud spacing of 400, 200, 100, and 50 mm from top to bottom.

difference in the moment of inertia and on the experimental results. Therefore, this so-called modified cross section was considered as a new case, and the corresponding change in the behavior of the composite beam was additionally observed. Figure 3 shows, respectively, the inverted-T steel girders installed with the forms for placing the UHPC slab and the completed test members. Figure 4 presents the setup for the loading test together with the layout of the sensors. Moreover, the literature reported that placing of UHPC from end of the member allowed better structural performance than placing UHPC at midspan of the member due to fluidity of UHPC mixture [15]. It affects orientation of the steel fibers in a longitudinal direction parallel to the flexural tensile stresses at midspan of the beam. Therefore, the UHPC mixture in this study was placed from end of the member to center. The fibers in the UHPC mix were added into the mixer with small amounts by hands to prevent lumps in the mixture.

2.2.2. Shear Connector and Steel Girder. Two types of studs are adopted (Figure 2(e)). Both types have identical height of 50 mm with respective shank diameter and head diameter of 13 and 22 mm (Detail B) and 18.5 and 34 mm (Detail A). The choice to use two types of studs was done to fit with the different performances developed by the 180 MPa UHPC mix and the 120 MPa and 150 MPa UHPC mixes. From the direct tensile test, the yield strength and the ultimate strength of the shear connector are found to be 371 MPa and 472 MPa, respectively. Besides, the steel girder is made of structural steel SM490. Referring to the data provided by the manufacturer, the yield strength and ultimate strength of the steel girder are 397 MPa and 550 MPa, respectively.

3. Test Results and Discussion

3.1. Crack and Failure Patterns. Table 3 summarizes the crack and failure patterns observed during the 3-point

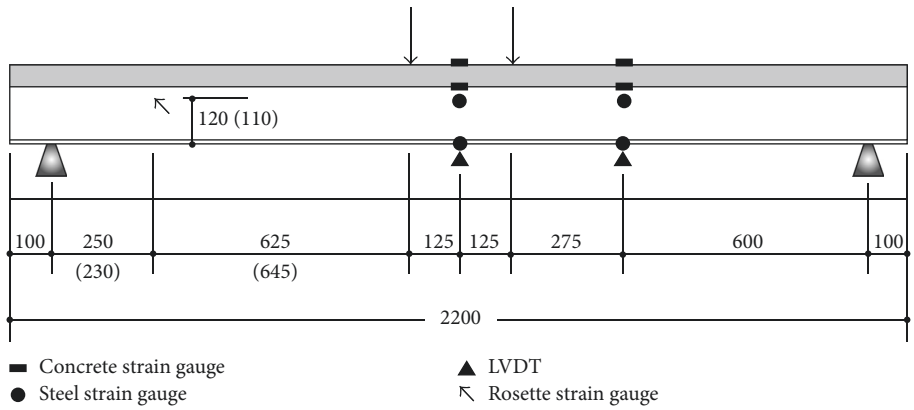

Figure 4: Loading test setup and sensor layout [12].

Table 3: Crack and failure patterns of test members.

Test member	Occurrence of longitudinal crack on slab	Crack on lateral face of slab				Failure pattern
		Extension from midspan (mm)	Number of cracks	Crack width (mm)	Pattern	
120f-50-50	No	200	4	0.01	C	Flexural compression
120f-50-100	No	—	—	—	—	
120f-50-200	Yes	100	4	0.01	T	Flexural compression + failure of concrete around stud
120f-50-400	Yes	100	3	0.01	T	
120f-100-50	No	400	8	0.02	T	Flexural compression
120f-100-100	No	200	4	0.02	T	
120f-100-200	Yes	400	5	0.02	T	Flexural compression + failure of concrete around stud
120f-100-400	Yes	600	8	0.02	T	
150f-50-50	No	100	5	0.01	C	Flexural compression
150f-50-100	No	—	—	—	—	
150f-50-200	Yes	—	—	—	—	Flexural compression + failure of concrete around stud
150f-50-400	Yes	200	10	0.01	C	
150f-100-50	No	400	6	0.02	T	Flexural compression
150f-100-100	No	400	5	0.02	T	
150f-100-200	Yes	400	5	0.02	T	Flexural compression + failure of concrete around stud
150f-100-400	Yes	400	8	0.02	T	
180f-50-50	No	Center	4	0.02		Flexural compression
180f-50-100	Yes	400	8	0.02		
180f-50-200	Yes	800	18	0.02		Flexural compression + failure of concrete around stud
180f-50-400	Yes	400	10	0.02		
180f-100-50	No	1000	13	0.02		Flexural compression
180f-100-100	No	1000	22	0.02		
180f-100-200	No	1000	13	0.02		Flexural tension
180f-100-400	No	800	20	0.03		

loading test of the test beams, and their representative pictures are shown in Figure 5. In Table 3, C stands for compression failure and cracking, and T for crack on tensile area.

Thinner slab thickness and larger stud spacing eased the occurrence of axial cracks on the top face of the slab. These cracks can be attributed to the tensile stresses developed through the redistribution of the force concentrated in a small area around the stud to the neighboring concrete [16]. Concretely, the 120 MPa and 150 MPa members with stud spacing larger than 200 mm experienced axial cracking on the top face of the slab regardless of the slab thickness. Except member 180f-50-100, axial cracking occurred only for the 180 MPa members with slab thickness of 50 mm and stud spacing larger than 200 mm. This observation may indicate that stable composite behavior without occurrence of axial cracking on the top face of the slab would be achieved with stud spacing shorter than 200 mm and high compressive strength of UHPC or thick UHPC slab.

The 120 MPa members failed through compression of concrete immediately after yielding of steel. The 150 MPa members showed postyielding ductile behavior before failure through compression of concrete. However, spalling of the connection of the stud occurred in the members with stud spacing larger than 200 mm and regardless of the compressive strength. Moreover, significant degradation of the ultimate load is observed for stud spacing of 400 mm. On the other hand, for the 180 MPa members with slab

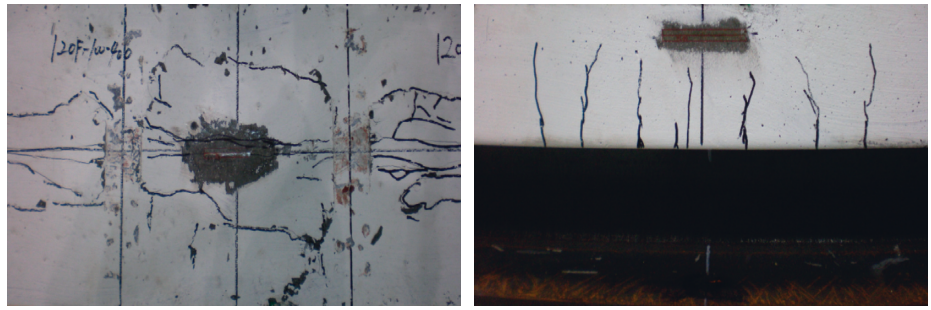

Top face of slab Side face of slab

(a)

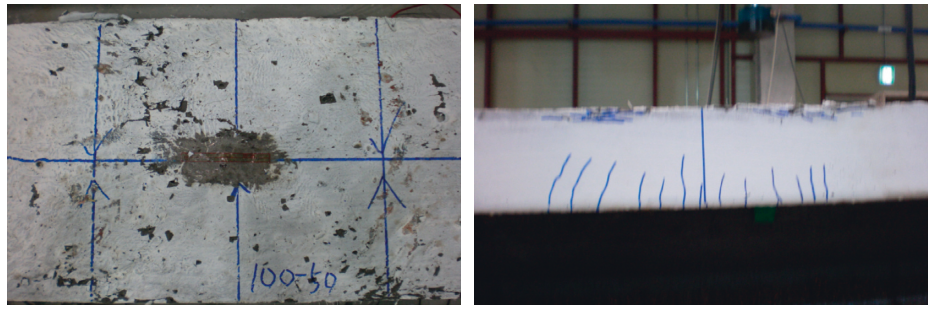

Top face of slab Side face of slab

(b)

Figure 5: Crack pattern of the specimens: (a) member 120f-100-400; (b) member 180f-100-50.

thickness of 50 mm, concrete failure occurred through tension for stud spacing of 400 mm and, through compression for stud spacing smaller than 200 mm. For the 180 MPa test members with slab thickness of 100 mm, failure of concrete occurred through flexure for stud spacing of 400 mm and through compression for stud spacing smaller than 200 mm.

3.2. Load-Displacement Curves. Figure 6 plots the load-displacement curves measured during the bending test of the composite beams. The ultimate load is seen to increase with thicker slab thickness and shorter stud spacing. Except the 180 MPa members with slab thickness of 100 mm, all the test members experienced compressive failure of the top layer concrete. This situation rendered it impossible to evaluate the effect of the difference in the amount of steel fiber on the tensile strength of concrete.

Eurocode-4 [17, 18] defines the characteristic relative slip, δ_{uk} as $0.9\delta_u$, where δ_u is the relative slip measured at load P_{RK} corresponding to the ultimate load reduced by 10%. Eurocode-4 assesses ductile behavior when this characteristic relative slip is larger than 6 mm and states that stable behavior is achieved by the composite member in such case. For comparison with the stipulations of Eurocode-4 [17], Table 4 arranges the yield load at the bottom flange of the steel girder, the ultimate load, the failure load, the relative slip at 90% of the failure load, and the characteristic relative slip measured in the tests.

In view of Table 4, the test members, except member 120f-50-400, are seen to develop characteristic relative slip ranging between 7.32 and 15.16 mm. This indicates that all the specimens develop sufficient ductile behavior since these values exceed significantly the ductile behavior limit of 6 mm recommended in Eurocode-4.

Member 120f-50-400 with thin slab, the largest stud spacing and the lowest compressive strength of UHPC among the considered mixes presents the most unfavorable conditions in term of structural resistance. Despite such weakness, this member experiences a characteristic relative slip of 5.36 mm that is slightly inferior to the 6 mm ductile behavior limit of Eurocode-4. This limit can be satisfied easily through slight modification of the inverted-T steel girder.

3.3. Load-Strain Curves of UHPC Slab. Figures 7 and 8 plot the load-concrete strain curves at the top and bottom of the slab. The ultimate compressive strain of the UHPC slab is approximately 0.004, which is in good agreement with the results of previous studies on the material behavior of UHPC [12, 19, 20]. It can also be observed that the structural performance degrades with larger stud spacing because of the debonding of concrete around the stud before the development of the UHPC material capacity.

For the test members with slab thickness of 50 mm, compressive strain is developed at the bottom of the slab at early loading due to the position of the neutral axis in the web of the steel girder. With the increase of the load, debonding of the shear connection at midspan occurred, and the members started to show noncomposite behavior resulting in the development of tensile strain at the bottom of the slab.

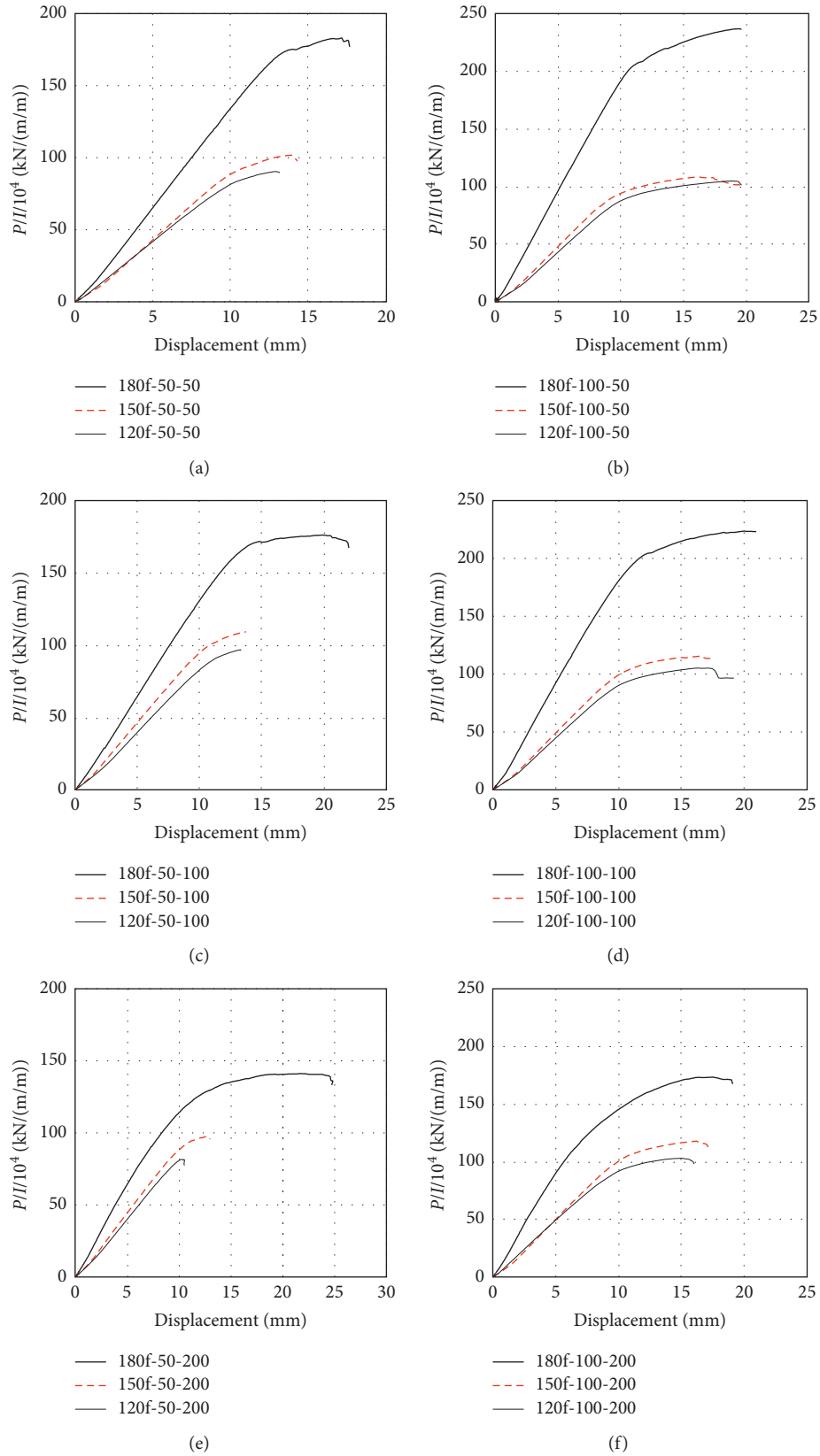

Figure 6: Continued.

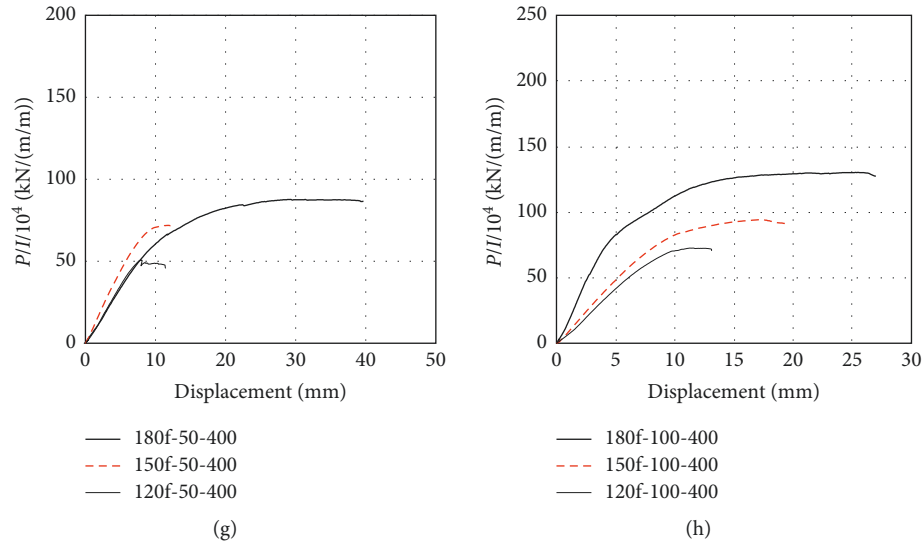

Figure 6: Load-displacement curves for the specimens. (a) Slab thickness, stud spacing (50 mm, 50 mm); (b) slab thickness, stud spacing (100 mm, 50 mm); (c) slab thickness, stud spacing (50 mm, 100 mm); (d) slab thickness, stud spacing (100 mm, 100 mm); (e) slab thickness, stud spacing (50 mm, 200 mm); (f) slab thickness, stud spacing (100 mm, 200 mm); (g) slab thickness, stud spacing (50 mm, 400 mm); (h) slab thickness, stud spacing (100 mm, 400 mm).

Table 4: Yield, ultimate and failure load, and characteristic slip measured in the loading test.

Test member	Yield load (kN)	Ultimate load (kN)	Failure load (kN)	δ_u (mm)	δ_{uk} (mm)
120f-50-50	554.1	585.5	580.0	9.82	8.84
120f-50-100	473.3	589.5	585.6	10.53	9.48
120f-50-200	—	497.1	471.6	8.41	7.57
120f-50-400	—	302.4	284.8	5.96	5.36
120f-100-50	500.2	702.6	678.5	10.82	9.74
120f-100-100	572.0	666.6	611.8	9.52	8.57
120f-100-200	585.0	647.2	615.9	9.45	8.51
120f-100-400	462.9	468.8	456.1	8.26	7.43
150f-50-50	490.1	625.0	579.9	9.51	8.56
150f-50-100	598.2	631.5	631.5	10.50	9.45
150f-50-200	473.6	557.9	548.1	9.71	8.74
150f-50-400	—	418.0	416.6	8.13	7.32
150f-100-50	555.9	684.3	630.4	9.22	8.30
150f-100-100	595.5	691.9	676.8	10.37	9.33
150f-100-200	536.9	699.6	653.5	9.86	8.87
150f-100-400	—	570.7	543.5	9.64	8.68
180f-50-50	428.1	573.2	554.2	11.72	10.54
180f-50-100	431.0	550.9	522.9	11.70	10.53
180f-50-200	408.7	450.9	425.3	10.87	9.78
180f-50-400	278.9	281.4	277.4	16.84	15.16
180f-100-50	567.2	807.4	806.4	12.28	11.05
180f-100-100	558.7	755.8	752.4	11.70	10.53
180f-100-200	535.9	583.2	563.2	10.77	9.69
180f-100-400	—	435.4	425.6	10.45	9.41

Besides, the test members with slab thickness of 100 mm developed tensile strain at the bottom of the concrete slab from early loading to failure due to the position of the neutral axis at the level of the concrete slab.

3.4. Load-Strain Curves of Inverted-T Steel Girder. Figure 9 plots the load-strain curves at the flange of the inverted-T steel girder. The yield strain of the steel girder remains below 0.002, which is in good agreement with the tensile test results of the material [12, 19, 20]. Here also, it can be observed that the structural performance degrades with larger stud spacing because of the debonding of concrete around stud before the development of the UHPC material capacity.

Unlike the other test members, member 180f-100-50 underwent failure without yielding. This peculiar behavior seems to be due to the large thickness and excessively

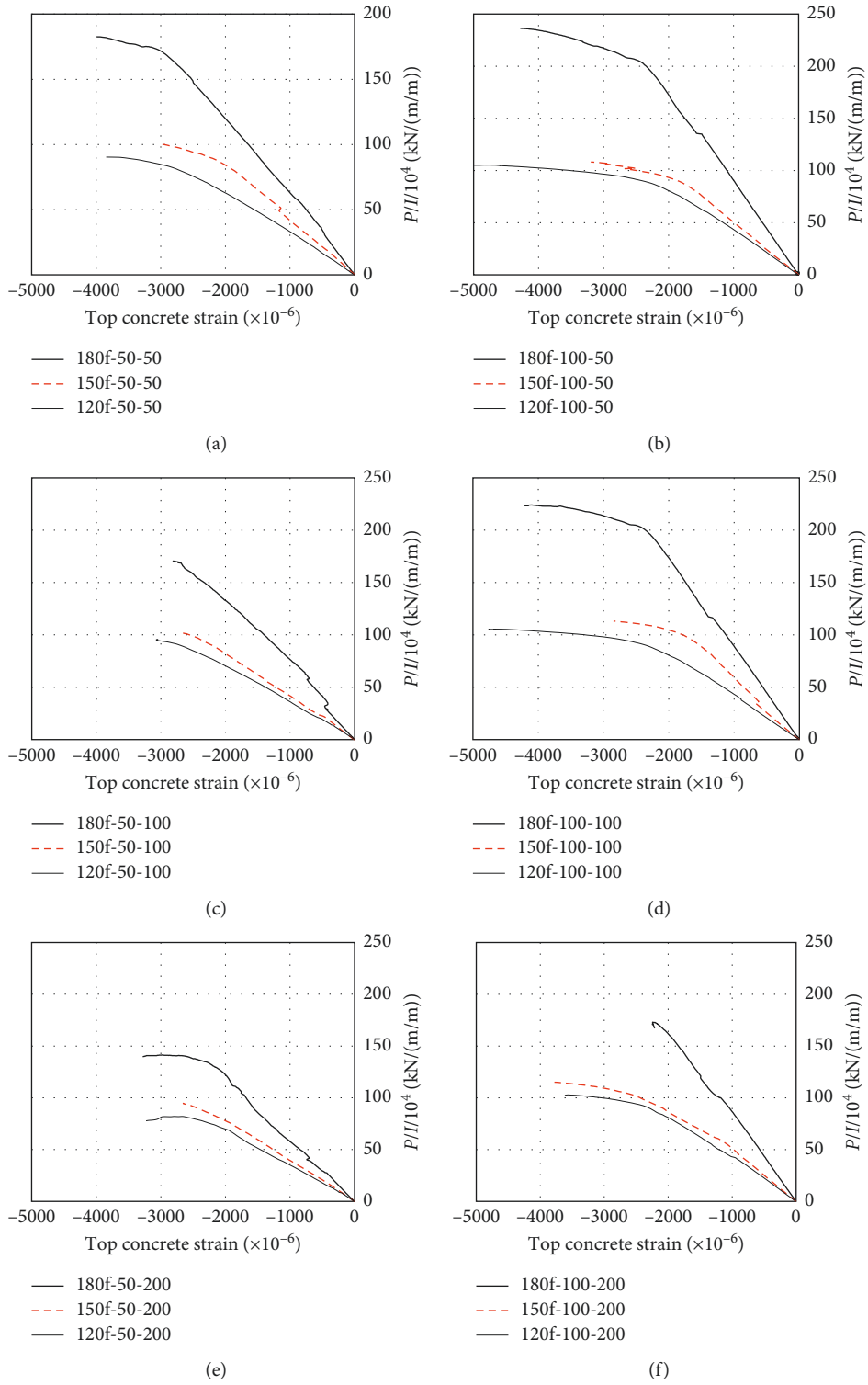

Figure 7: Continued.

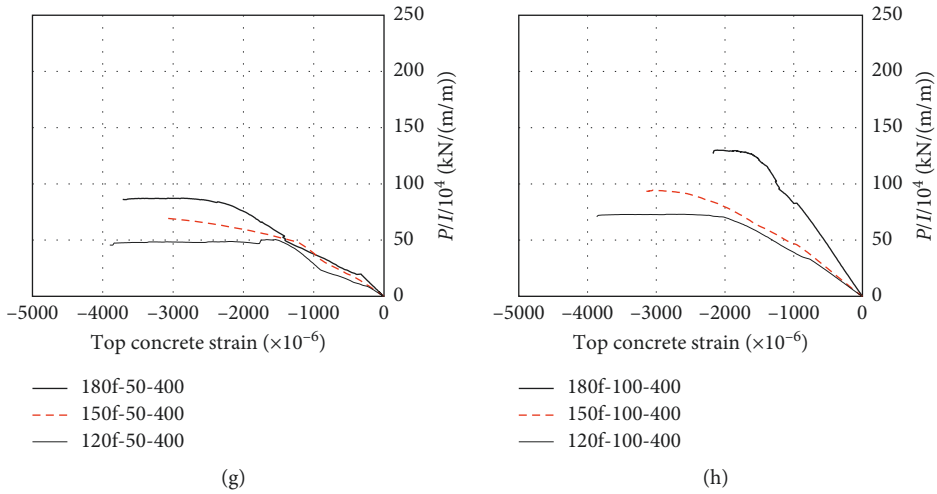

(g) (h)

Figure 7: Load-concrete strain curves at top of slab for the specimens. (a) Slab thickness, stud spacing (50 mm, 50 mm); (b) slab thickness, stud spacing (100 mm, 50 mm); (c) slab thickness, stud spacing (50 mm, 100 mm); (d) slab thickness, stud spacing (100 mm, 100 mm); (e) slab thickness, stud spacing (50 mm, 200 mm); (f) slab thickness, stud spacing (100 mm, 200 mm); (g) slab thickness, stud spacing (50 mm, 400 mm); (h) slab thickness, stud spacing (50 mm, 400 mm).

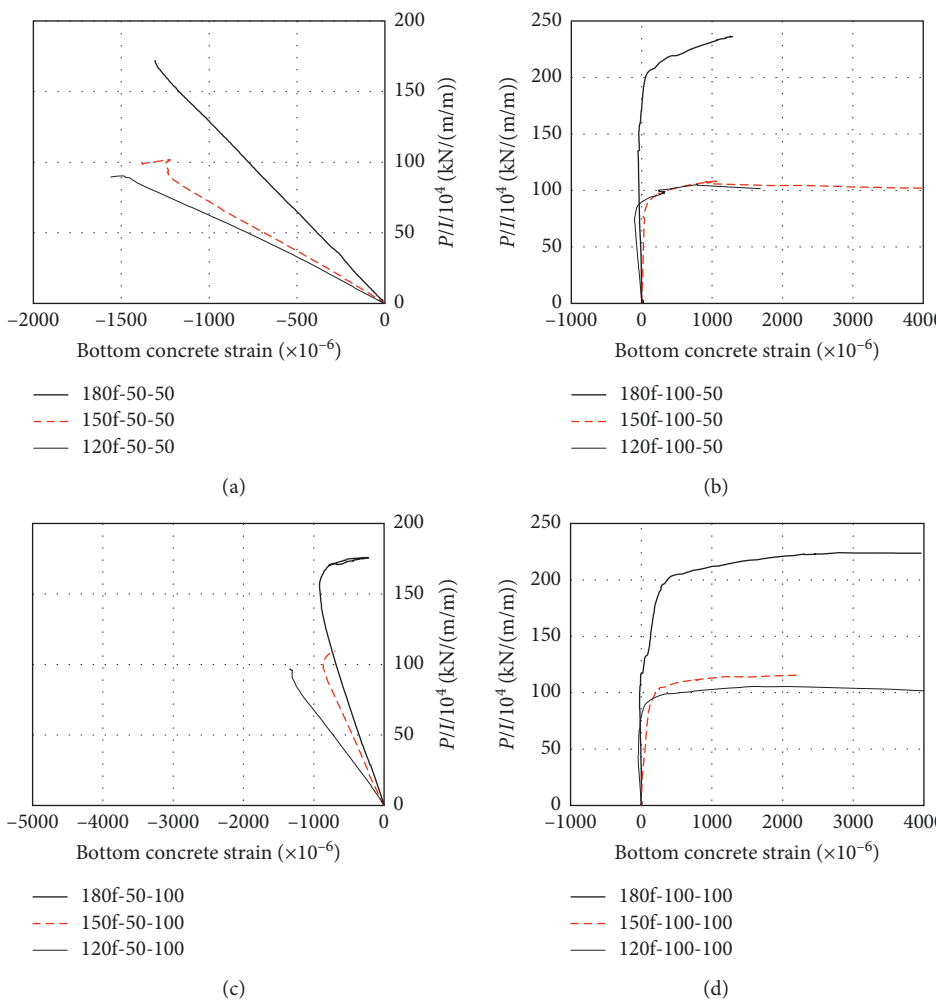

(a) (b)

(c) (d)

Figure 8: Continued.

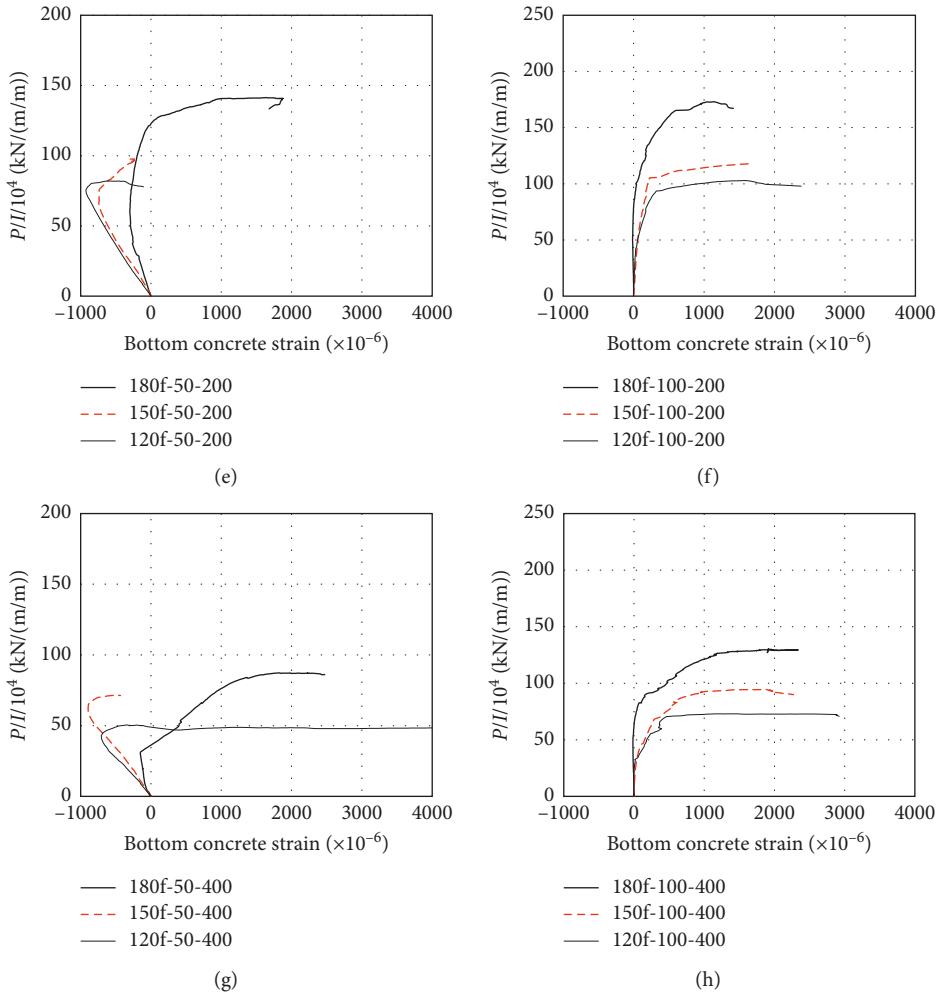

Figure 8: Load-concrete strain curves at bottom of slab for the specimens. (a) Slab thickness, stud spacing (50 mm, 50 mm); (b) slab thickness, stud spacing (100 mm, 50 mm); (c) slab thickness, stud spacing (50 mm, 100 mm); (d) slab thickness, stud spacing (100 mm, 100 mm); (e) slab thickness, stud spacing (50 mm, 200 mm); (f) slab thickness, stud spacing (100 mm, 200 mm); (g) slab thickness, stud spacing (50 mm, 400 mm); (h) slab thickness, stud spacing (50 mm, 400 mm).

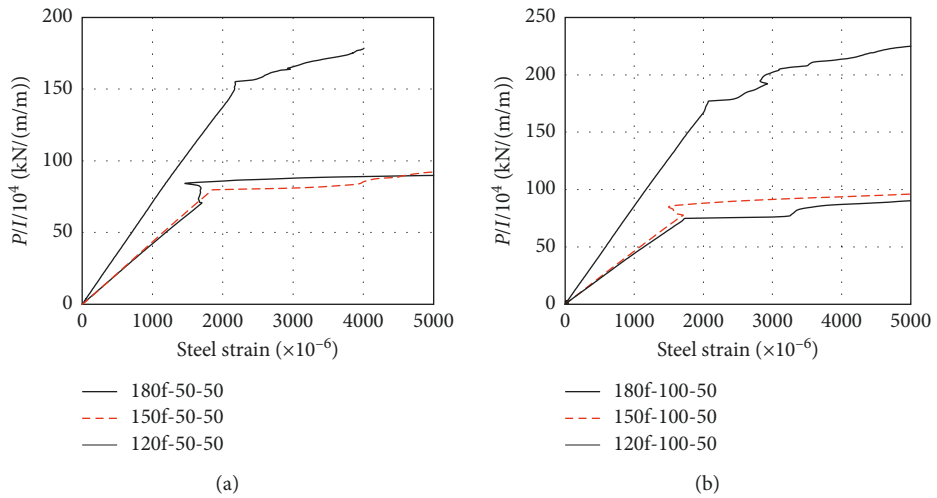

Figure 9: Continued.

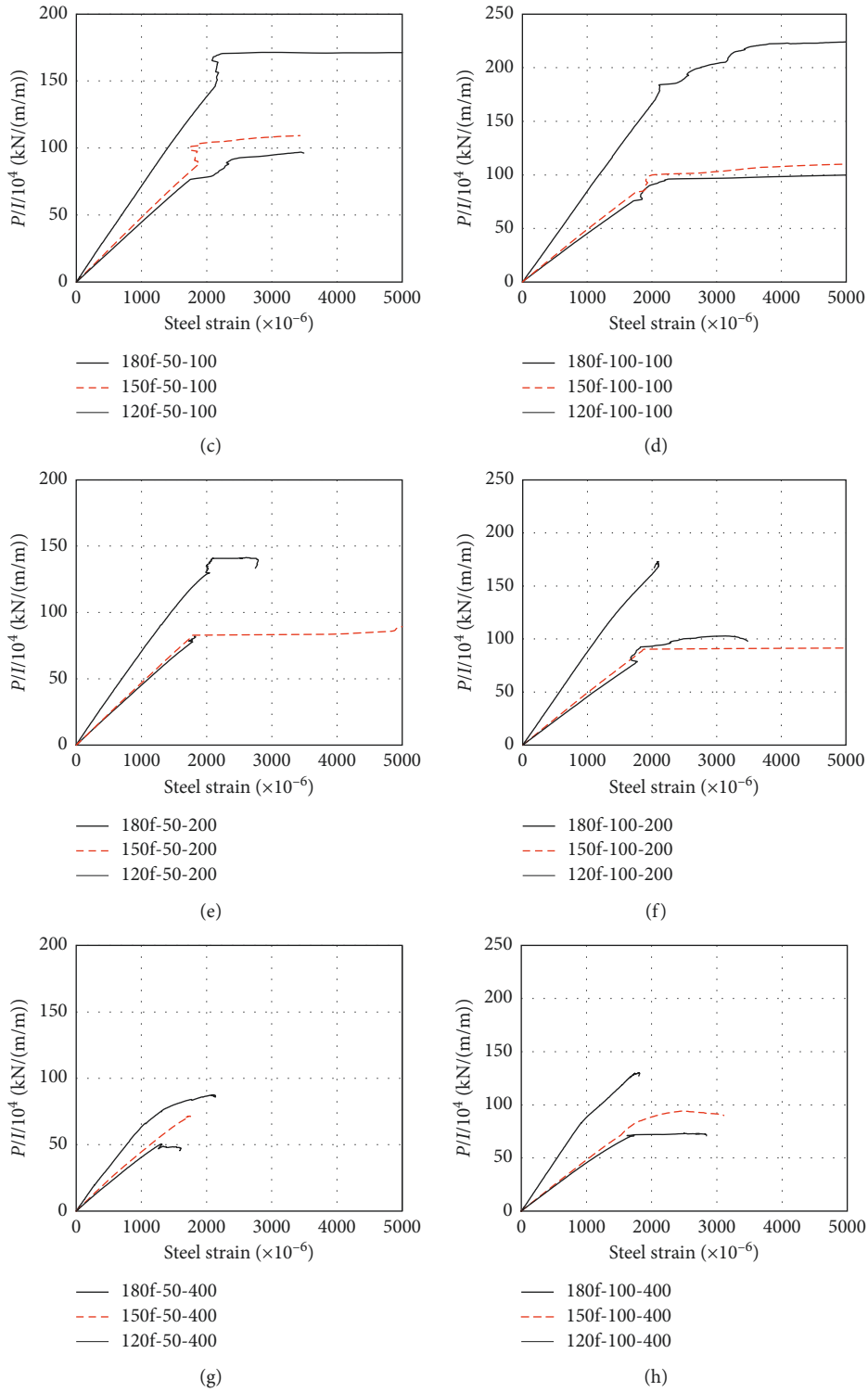

Figure 9: Load-strain curves at bottom flange of steel girder. (a) Slab thickness, stud spacing (50 mm, 50 mm); (b) slab thickness, stud spacing (100 mm, 50 mm); (c) slab thickness, stud spacing (50 mm, 100 mm); (d) slab thickness, stud spacing (100 mm, 100 mm); (e) slab thickness, stud spacing (50 mm, 200 mm); (f) slab thickness, stud spacing (100 mm, 200 mm); (g) slab thickness, stud spacing (50 mm, 400 mm); (h) slab thickness, stud spacing (50 mm, 400 mm).

dense arrangement of the studs, which made the compressive failure of the concrete slab occur prior to the debonding of concrete around stud or yielding of steel girder [12].

Similar behavior can be observed for members 180f-100-400, 120f-50-200, 120f-50-400, 150f-50-400, and 150f-100-400. For these members, the reason can be attributed to large thickness and excessively scattered arrangement of the studs,

Table 5: Comparison of experimental ultimate horizontal shear force and predicted shear strength without safety factor.

Test member	a: horizontal shear force by test (kN)	b: stud force by (1) (kN)	a/b	c: stud force by (5) (kN)	a/c
120f-50-50	1,386	2,535	0.55	4,636	0.30
120f-50-100	1,138	1,268	0.90	2,318	0.49
120f-50-200	965	634	1.52	1,159	0.83
120f-50-400	533	317	1.68	579	0.92
120f-100-50	1,937	2,535	0.76	4,636	0.42
120f-100-100	1,399	1,268	1.10	2,318	0.60
120f-100-200	1,016	634	1.60	1,159	0.88
120f-100-400	753	317	2.38	579	1.30
150f-50-50	1,151	2,785	0.41	5,093	0.23
150f-50-100	1,041	1,393	0.75	2,547	0.41
150f-50-200	803	696	1.15	1,273	0.63
150f-50-400	1,089	348	3.13	637	1.71
150f-100-50	1,100	2,785	0.39	5,093	0.22
150f-100-100	900	1,393	0.65	2,547	0.35
150f-100-200	1,365	696	1.96	1,273	1.07
150f-100-400	852	348	2.45	637	1.34
180f-50-50	1,206	799	1.51	998	1.21
180f-50-100	997	399	2.50	499	2.00
180f-50-200	564	200	2.83	250	2.26
180f-50-400	347	100	3.48	125	2.78
180f-100-50	1,686	799	2.11	998	1.69
180f-100-100	1,125	399	2.82	499	2.26
180f-100-200	824	200	4.13	250	3.30
180f-100-400	528	100	5.29	125	4.23
Average	—	—	1.92	—	1.31

which made the concrete slab fail through noncomposite and compression-flexure prior to the debonding of concrete around the stud.

3.5. Evaluation of Shear Connector by Horizontal Shear Force. Eurocode-4 [16, 17] recommends the smallest value between (1) and (2) be the design shear resistance of the headed shear connector.

$$P_{RD} = \frac{0.8 f_u \pi d^2}{4\gamma_v}, \quad (1)$$

$$P_{RD} = \frac{0.29 \alpha d^2 \sqrt{f_{ck} E_{cm}}}{\gamma_v}, \quad (2)$$

where γ_v = partial factor (1.25), d = stud shank diameter, f_u = specified ultimate tensile strength of the material of the stud, f_{ck} = compressive strength of concrete, and E_{cm} = elastic modulus of concrete, and

$$\alpha = 0.2\left(\frac{h_{sc}}{d} + 1\right) \quad \text{for } 3 \le h_{sc} < 4, \quad (3)$$

$$\alpha = 1 \quad \text{for } \frac{h_{sc}}{d} > 4, \quad (4)$$

where h_{sc} = overall nominal height of the stud.

Equation (5) expresses the nominal shear resistance of one stud shear connector embedded in the concrete deck recommended in AASHTO-LRFD [21].

$$Q_r = \phi_{sc} Q_n = \phi_{sc} 0.5 A_{sc} \sqrt{f'_c E_c} \le \phi_{sc} F_u A_{sc}, \quad (5)$$

where ϕ_{sc} = resistance factor, A_{sc} = cross-sectional area of stud, E_c = modulus of elasticity of concrete, and F_u = minimum specified tensile strength of one stud.

The horizontal shear force working on the slab calculated indirectly using the concrete strains measured at the top and bottom of the slab and the static strength of the stud calculated by means of (1)–(5) of Eurocode-4 [18] and AASHTO-LRFD [21] are compared in Table 5. Here, the static strength of the stud obtained by (1)–(5) represents the physical resistance of the stud itself owing to the outstanding performance of UHPC [12].

Figure 10 plots the load-horizontal shear force curves of the specimens. As a matter of fact, the horizontal shear force becomes larger with thicker slab and denser arrangement of the studs [12]. The comparison of the ultimate shear force of the test members and the static strengths of the stud given by the design formulae in (1)–(5) reveals that the average ratio is 1.92 for Eurocode-4 and 1.31 for AASHTO-LRFD.

The members with large stud spacing of 200 and 400 mm exhibited larger values than those provided by the design formulae. After the noncomposite behavior, the UHPC slab and the stud developed higher ultimate strength than the expected resistance. The members with stud spacing shorter than 100 mm experienced sudden failure through flexure before the stud could develop its proper capacity.

In Table 5, the comparison of the experimental and predicted shear resistances with respect to the stud spacing shows that the ratio of the experimental shear force to the design shear strength increases with thicker slab and larger stud spacing. This can be explained by the reduction of the horizontal shear force caused by the noncomposite behavior

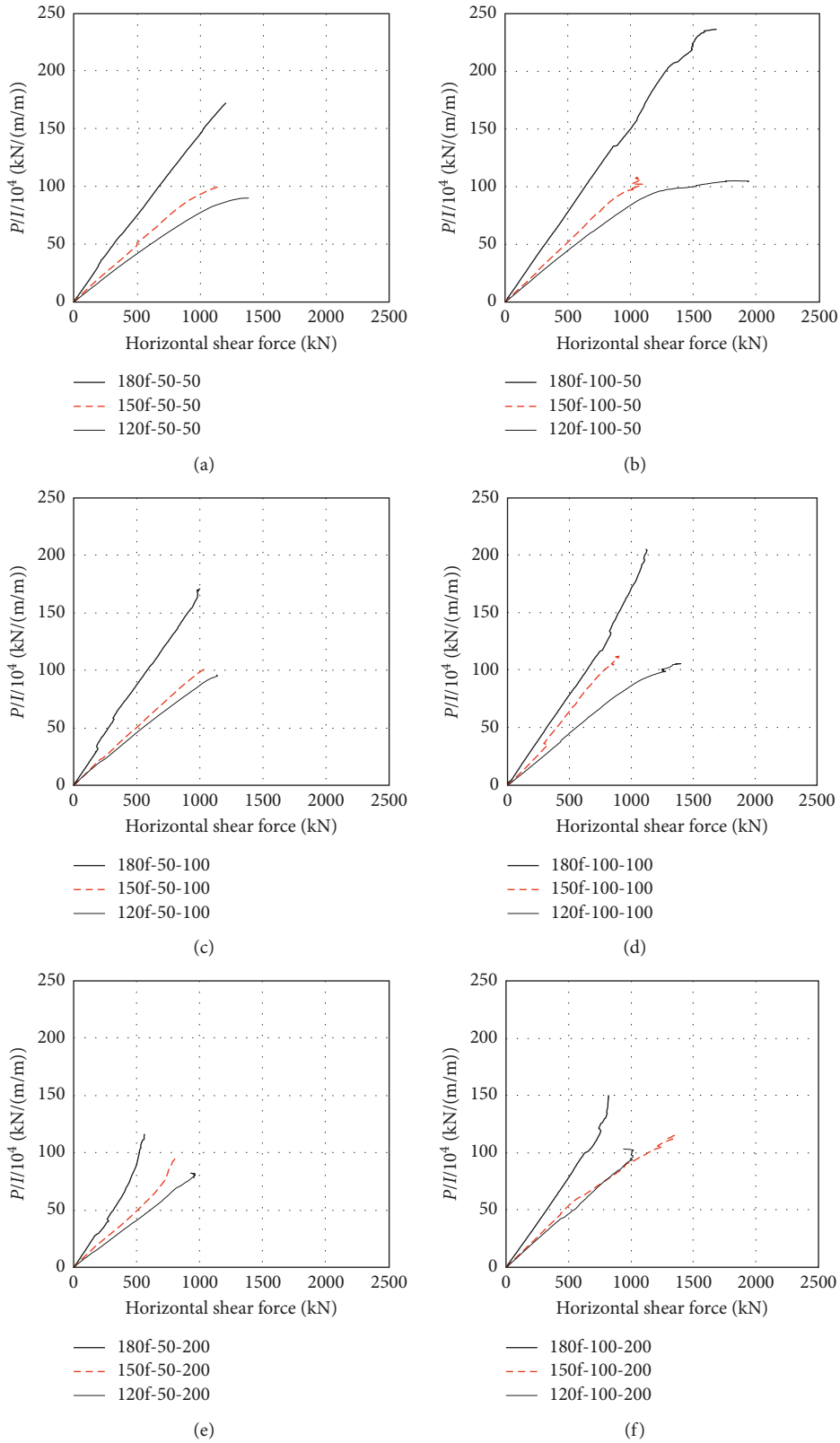

Figure 10: Continued.

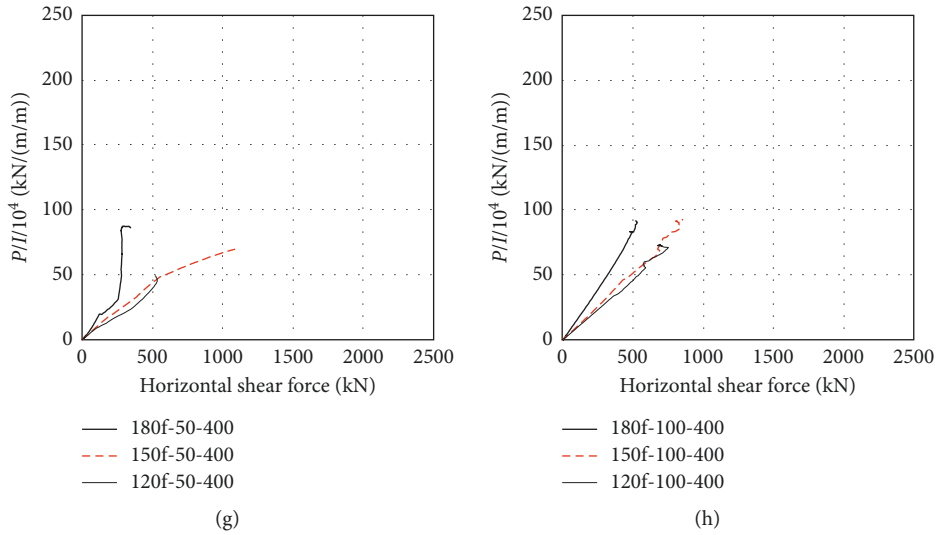

Figure 10: Load-horizontal shear force curves. (a) Slab thickness, stud spacing (50 mm, 50 mm); (b) slab thickness, stud spacing (100 mm, 50 mm); (c) slab thickness, stud spacing (50 mm, 100 mm); (d) slab thickness, stud spacing (100 mm, 100 mm); (e) slab thickness, stud spacing (50 mm, 200 mm); (f) slab thickness, stud spacing (100 mm, 200 mm); (g) slab thickness, stud spacing (50 mm, 400 mm); (h) slab thickness, stud spacing (100 mm, 400 mm).

resulting from larger stud spacing. The reason for the larger experimental results obtained for thicker slabs can be found in the fact that the current design formulae assume the static strength of the stud to be the resistance of the stud itself in the case where UHPC develops outstanding performance. This implies that the current design formulae cannot reflect the thickness of the slab for high performance concretes like UHPC. In the future, improved design formulae should be derived based upon experimental data for high performance concretes like UHPC. Note that, future studies should be additionally conducted on full-scale specimens since the specifications of Eurocode-4 [17, 18] and AASHTO-LRFD [21] used for the comparison in this study cannot consider the scale effect produced by cyclic loading and scaled specimens.

4. Conclusions

The following conclusions can be drawn based on the experimental results:

(1) Larger stud spacing with thin slab eased the occurrence of axial cracks along the steel girder at the top face of the slab. The occurrence of these axial cracks could be attributed to the tensile stress generated by the redistribution of the load concentrated in a small area around the stud to the wider neighboring concrete.

(2) The composite beam specimens developed sufficient ductile behavior since the characteristic relative slip ranging between 7.32 and 15.16 mm exceeded significantly the ductile behavior limit of 6 mm stipulated in Eurocode-4.

(3) The horizontal shear force increased with thicker slab and denser arrangement of the studs. The comparison of the ultimate horizontal shear force of the test members and the static strengths of the stud given by design codes revealed that the experimental results were larger by 1.92 and 1.31 times than the predictions of Eurocode-4 and AASHTO-LRFD, respectively. The members with large stud spacing exhibited larger values than those predicted by the design formulae. After the noncomposite behavior, the UHPC slab and the stud developed higher ultimate strength than the expected resistance. The members with short stud spacing experienced sudden failure through flexure before the stud could develop its proper capacity.

(4) The thickness of the slab could not be reflected by the current design formulae of Eurocode-4 and AASHTO-LRFD in the case of high performance concretes like UHPC. Improved design formulae should be derived in the future based upon experimental data for high performance concretes like UHPC.

Conflicts of Interest

The authors declare that there are no conflicts of interest regarding the publication of this paper.

Acknowledgments

This research was financially supported by the Korean Ministry of Environment as "Public Technology Program Based on Environmental Policy" (2016000700003). And this research was also financially supported by a grant (13SCIPA02) from the Smart Civil Infrastructure Research Program funded by the Ministry of Land, Infrastructure and Transport (MOLIT) of the Korean government and Korea Agency for Infrastructure Technology Advancement (KAIA).

References

[1] H. G. Russell and B. A. Graybeal, *Ultra-High Performance Concrete: A State-of-the-Art Report for the Bridge Community*, US Department of Transportation, Federal Highway Administration, Washington, DC, USA, Publication No. FHWA-HRT-13-060, 2013.

[2] H. John, *The Implementation of Full Depth UHPC Waffle Bridge Deck Panels: Final Report*, Publication no. FHWA-HIF-13-031, US Department of Transportation, Federal Highway Administration, Washington, DC, USA, 2013.

[3] A. E. Naaman and K. Chandrangsu, "Innovative bridge deck system using high-performance fiber-reinforced cement composites," *ACI Structural Journal*, vol. 101, no. 1, pp. 57–64, 2004.

[4] K. Wille and G. Parra-Montesinos, "Effect of beam size, casting method, and support conditions on flexural behavior of ultra-high-performance fiber-reinforced concrete," *ACI Materials Journal*, vol. 109, no. 3, pp. 379–388, 2012.

[5] I. H. Yang, C. Joh, and B. S. Kim, "Flexural strength of large-scale ultra high performance concrete prestressed T-beams," *Canadian Journal of Civil Engineering*, vol. 38, no. 11, pp. 1185–1195, 2011.

[6] B. A. Graybeal, "Flexural behavior of an ultra high performance concrete I-girder," *Journal of Bridge Engineering*, vol. 13, no. 6, pp. 602–610, 2008.

[7] Y. Yao, X. Wang, and B. Mabasher, "Flexural design procedures for UHPC beams and slabs," in *Proceedings of the First International Interactive Symposium on UHPC*, pp. 1–10, Des Moines, IA, USA, 2016.

[8] D. Y. Yoo and Y. S. Yoon, "A review on structural behavior, design, and application of ultra-high-performance fiber-reinforced concrete," *International Journal of Concrete Structures and Materials*, vol. 10, no. 2, pp. 125–142, 2016.

[9] European Commission, *EUR 25321–Prefabricated Enduring Composite Beams Based on Innovative Shear Transmission (Preco-Beam), RFSR-CT-2006–00030, Final Report*, European Commission, Brussels, Belgium, 2009.

[10] W. Dudziński, G. Pękalski, P. Harnatkiewicz et al., "Study on fatigue cracks in steel-concrete shear connection with composite dowels," *Archives of Civil and Mechanical Engineering*, vol. 11, no. 4, pp. 839–858, 2011.

[11] K. C. Lee, C. Joh, E. S. Choi, and J. S. Kim, "Stud and puzzle-strip shear connector for composite beam of UHPC deck and inverted-T steel girder," *Journal of the Korea Concrete Institute*, vol. 26, no. 2, pp. 151–157, 2014.

[12] S. W. Yoo and J. F. Choo, "Evaluation of the flexural behavior of composite beam with inverted-T steel girder and steel fiber reinforced ultra high performance concrete slab," *Engineering Structures*, vol. 118, pp. 1–15, 2016.

[13] Korea Concrete Institute, *Design Recommendations for Ultra-High Performance Concrete K-UHPC. KCI-M-12–003*, Korea Concrete Institute, Seoul, Republic of Korea, 2012.

[14] S. T. Kang and G. S. Ryu, "The effect of steel-fiber contents on the compressive stress-strain relation of ultra high performance cementitious composites (UHPCC)," *Journal of the Korea Concrete Institute*, vol. 23, no. 1, pp. 67–75, 2011.

[15] S. J. Barnett, J. F. Lataste, T. Parry, S. G. Millard, and M. N. Soutsos, "Assessment of fibre orientation in ultra high performance fibre reinforced concrete and its effect on flexural strength," *Materials and Structures*, vol. 43, no. 7, pp. 1009–1023, 2010.

[16] S. W. Yoo, Y. S. Ahn, Y. D. Cha, and C. Joh, "Experiment of flexural behavior of composite beam with steel fiber reinforced ultra high performance concrete deck and inverted-T steel girder," *Journal of the Korea Concrete Institute*, vol. 26, no. 6, pp. 761–769, 2014.

[17] European Committee for Standardization, *CEN 1994-4-4. Eurocode-4: Design of Composite Steel and Concrete Structures, Part 1-1: General Rules and Rules for Buildings*, CEN, Brussels, Belgium, 2004.

[18] European Committee for Standardization, *CEN 1994-2. Eurocode-4: Design of Composite Steel and Concrete Structures, Part 2: General Rules and Rules for Bridges*, CEN, Brussels, Belgium, 2005.

[19] M. Feldman, O. Hechler, J. Hegger, and S. Rauscher, "Fatigue behavior of shear connectors in high performance concrete," in *Proceedings of the International Conference on Composite Construction in Steel and Concrete VI*, pp. 78–91, Tabernash, CO, USA, July 2008.

[20] J. S. Park, Y. J. Kim, J. R. Cho, and S. J. Jeon, "Characteristics of strength development of ultra-high performance concrete according to curing condition," *Journal of the Korea Concrete Institute*, vol. 25, no. 3, pp. 295–304, 2013.

[21] American Association of State Highway and Transportation Officials, *AASHTO LRFD Bridge Design Specifications*, AASHTO, Washington, DC, USA, 4th edition, 2007.